Journal of Metals, Materials and Minerals, 36(4), e2657, 2026

Physicochemical characterization and *in vitro* biocompatibility assessment of hydrothermally synthesized hydroxyapatite from oyster shells

Amin Saiff JOHARI[1,2,3], Nur Ayunie ZULKEPLI[1,2,*], Nur Shahida KADER BASHAH[3], Fatimah SALIM[1], Muhamad Hazri OTHMAN[3], and Nurazilah Mohd ZAINON[3]

[1] *Atta-Ur-Rahman Institute for Natural Product Discovery (AuRIns), Universiti Teknologi MARA (UiTM), Selangor Branch, Puncak Alam Campus, Selangor, 42300, Malaysia*

[2] *Centre for Medical Laboratory Technology Studies, Faculty of Health Sciences, Universiti Teknologi MARA (UiTM) Selangor Branch, Puncak Alam Campus, Selangor, 42300, Malaysia*

[3] *Advanced Materials Research Centre (AMREC), SIRIM Industrial Research, SIRIM Berhad, Kulim, Kedah, 09000, Malaysia*

***Corresponding author e-mail**: nayunie@uitm.edu.my

Received date:
15 February 2026
Revised date:
27 April 2026
Accepted date:
7 May 2026

Keywords:
Hydroxyapatite;
Oyster shells;
Hydrothermal;
Biocompatibility;
Saos-2

Abstract

Naturally produced Hydroxyapatite (HAP) yields beneficial attributes with regards to its biological functions including cell compatibility, proliferation and osteoinduction. This study synthesized HAP from oyster shells as a calcium source with multiple hydrothermal reaction times including 1 h, 6 h and 24 h at 150°C. A wet precipitated control sample was produced at room temperature. Characterization using FTIR, XRD, SEM-EDX and BET were conducted, followed by a degradation analysis. Biocompatibility study of Oys-HAP was performed against Saos-2 osteoblast-like cells. The results showed nano scaled elongated and oval-shaped Oys-HAP particles with high crystallinity, beta-type carbonated, non-stoichiometric Ca/P ratio with a maximum surface area of 41.39 $m^2 \cdot g^{-1}$. Furthermore, Oys-HAP samples were non-toxic and significantly enhanced Saos-2 cell proliferation by 65.6% compared to the negative control. These findings demonstrate the potential of oyster shell-derived Oys-HAP as a sustainable and effective biomaterial for biomedical applications.

1. Introduction

Calcium phosphate (CaP)-based biomaterials are among the most widely studied materials for biomedical applications. Hydroxyapatite (HAP), $Ca_{10}(PO_4)_6(OH)_2$, is a major component of the mineral phase of human bone and enamel and has been extensively used in orthopedic and dental applications due to its excellent biocompatibility, bioactivity, and ability to regulate cellular behavior. Its close resemblance to natural hard tissues further supports its suitability for regenerative and restorative purposes [1-3]. Despite its excellent properties, most commercial HAP products are synthesized using chemical precursors through energy-intensive processes, raising concerns about cost, environmental impact, and sustainability. Naturally derived biomaterials are gaining interest due to their abundance and potential for sustainable sourcing. In many cases, naturally derived materials have demonstrated improved performance in specific biomedical applications compared to their synthetic counterparts [4]. To address these limitations, research interest has shifted towards biogenic sources rich in calcium carbonate ($CaCO_3$), such as eggshells, mammalian bones, and marine shells. Among these, oyster shells represent an abundant and underutilized waste material generated by the seafood industry.

Several methods have been employed to produce HAP from biogenic sources, including wet chemical precipitation, sol–gel, and hydrothermal techniques. Wet precipitation is the simplest and most used method. However, it often results in HAP with lower crystallinity, purity, and yield compared to hydrothermal synthesis [5]. In contrast, the hydrothermal method is conducted under elevated temperature and pressure, promoting nucleation and crystal growth, and leading to highly crystalline, phase-pure HAP with controllable particle size and morphology [6]. In addition, this method offers relatively shorter reaction times. Previous studies have reported that hydrothermal treatment improves the crystallinity, morphology, and yield of oyster shell-derived HAP compared to conventional wet precipitation methods [7]. Nevertheless, optimization is still required, as hydrothermal synthesis is strongly influenced by parameters such as temperature, pH, and reaction time. Biocompatibility of biomaterials, involving direct or indirect contact with relevant cell types is an important step to assess its toxicity [8]. Although HAP is generally considered biocompatible, variations in synthesis methods can result in materials with different physicochemical properties, necessitating further biological evaluation, particularly for nanoscale HAP (nHAP) [9].

Accordingly, this study investigates the production of Oys-HAP from oyster shells using a direct hydrothermal method. The effects of reaction times (1H, 6H and 24H) on the physicochemical characteristics of the synthesized HAP are investigated. Furthermore, the cytocompatibility of the materials is evaluated through cell viability, proliferation, and adhesion assays using a Saos-2 osteoblast-like cell model, aiming to assess their potential for bone tissue engineering applications.

2. Experimental

2.1 Oyster shell source

The oyster shells were procured from a local Malaysian fishery. Oyster shells consisting of two different species, including *Crassostrea iredalei* and *Callionymus belcheri*, were collected from Ocean Rich Resources Sdn. Bhd., an industrial collaborator based in Sungai Merbok, Kedah, Malaysia which served as the foundational biomaterials for experimental processing.

2.2 Synthesis of oyster shells hydroxyapatite (Oys-HAP)

A method by [10] was adopted with modifications. The oyster shells were first cleaned with distilled water and rinsed at least 5 times to remove dirt or any sand present. The shells were dried completely in a 100°C oven (Binder, US) overnight. The dried shells were pulverized using an automated mortar (Retsch GmbH, US). The produced oyster shell powder (OSP) was sieved and kept in a dehumidifying cabinet prior to Oys-HAP synthesis. 2 g of OSP were mixed in a 20 mL solution of 25% (v/v) Hydrochloric Acid (HCL) and 95% Phosphoric Acid (H_3PO_4). The solution was left to stir continuously overnight at room temperature. Following complete mixing, 30% ammonium hydroxide (NH_3) solution was added gradually to turn the pH to 10. The reaction was quickly transferred to a hydrothermal vessel for the heat treatment as tabulated in Table 1. A control sample was prepared at room temperature without hydrothermal treatment.

2.3 Fourier transform infrared spectroscopy (FTIR) analysis

The functional groups of powdered samples were analyzed using a Fourier transform infrared (FT-IR) spectrometer (Perkin Elmer Spectrum 2000, USA). It is to determine the chemical profiles, or any phase transformations present in the samples. Powdered Oys-HAP was analyzed directly using the sampling point. For cleaning before a new sample was analyzed, 100% Acetone (Sigma Aldrich, USA) was used. The functional groups were analyzed with a wavenumber range of 600 cm^{-1} to 4000 cm^{-1} in range.

2.4 X-ray diffraction (XRD) analysis

The phase transformations and crystallinity of synthesized Oys-HAP samples was determined using an X-ray diffractometer (XRD); Bruker, D8 Advanced, Germany. The samples were be analyzed using Cu Kα radiation generated at 40 kV and 40 mA. The degrees of diffraction in samples were measured from 20°C to 50°C at a scanning speed of 5°C·min^{-1} and a step size of 0.02°. The crystallite size of powder samples was calculated using the Scherrer formula as described by [11]. For crystallinity, the value was calculated using a formula described by [12].

2.5 Field emission scanning electron microscope (FESEM-EDX) analysis

To obtain the morphological data (particle size and morphology) on the synthesized synthetic Oys-HAP samples, a scanning electron microscope (FESEM; Leo 1525, Germany) was used for analysis with a voltage of 20 kV. Before visualization, the sample is reconstituted with absolute ethanol. A carbon paper was immersed was the suspension containing Oys-HAP. The coated papers were first coated with platinum. The magnification used is 20,000X. An Energy Dispersive X-Ray Spectroscopy (EDX), Zeiss, Germany was used to measure the elements present in the samples.

2.6 Brunauer-Emmett-Teller (BET) analysis

The specific surface area (SSA) and pore size distributions of powdered Oys-HAP samples were measured through the multiple Brunauer–Emmett–Teller (BET) analysis that evaluates nitrogen adsorption-desorption isotherms at 77 K using Quantachrome Autosorb Automated Gas Sorption System Report Autosorb 1 Quantachrome Corporation.

2.7 Degradation analysis

The degradation behavior of Oys-HAP samples was carried out using a method described by [13] with minor modifications. The tests were performed in two solutions including Phosphate Buffer Saline (Oxoid, USA) and Simulated Body Fluid (SBF). The SBF solution was prepared by using a method by [14]. Briefly, 0.5 g of test samples were weighed and immersed in 20 mL of test solution. The test tubes were then transferred into a water bath (Lab Companion, Korea). The experiments were carried out at 37°C to simulate physiological conditions. The immersion times were carried out at 1, 3, 5, 7, and 14 days timepoints. The test solutions were refreshed every 2 days. At each set time point, the samples were filtered using a filter paper (GVS Filter Technology, Italy). After filtration, the samples were dried in an oven (Binder, Germany) at 100°C.

Table 1. The hydrothermal synthesis parameters employed in the preparation of oyster shells–derived hydroxyapatite (Oys-HAP).

Samples name/Code	Synthesis parameters	
	Hydrothermal (Time, Temperature)	Precipitation (Time, Temperature)
1H	1 h, 150°C	None
6H	6 h, 150°C	None
24H	24 h, 150°C	None
RT	None	1 h, Room Temperature
OSP	None	None

2.8 Cell culture

An *in vitro* model of Human Osteogenic Sarcoma cell line Saos-2 (iCell-h140, CellVers previously known as iCellBioScience, China) was used for the *in vitro* biocompatibility evaluation of Oys-HAP samples. Briefly, the cells were grown under the conditions of 5% CO_2 at 37°C. The cells were grown using high glucose Dulbecco Minimum Essential Medium (DMEM, Pricella, Elabscience, USA) with the supplementation of 10% Fetal Bovine Serum (Capricon Scientific, USA) and 1% of Antibiotic/Antimycotic solution (Capricon Scientific, USA). The cells were only subcultured when they reached about 80% confluency, which was checked microscopically using an inverted phase contrast microscope (Olympus IX73, Japan) routinely.

2.9 Biocompatibility analysis

The biocompatibility of Oy-HAP samples was assessed using an indirect cytotoxicity method in accordance with the standard for medical device evaluation [15]. Briefly, powder samples were immersed in 10 mL of complete cell culture media and incubated at 37°C in a humidified incubator (IC50 Memmert, Germany) for 72 h to obtain extraction media [16]. The resulting stock extract corresponded to an approximate concentration of 200 $mg \cdot mL^{-1}$, consistent with the recommended extraction ratio. Serial dilutions of the stock solution were subsequently prepared using complete culture medium to obtain at least four concentration levels. Confluent cells were detached using 0.25% Trypsin-EDTA solution (Nacalai Tesque, Japan) and seeded into a 96-well plate at a density of 1×10^4 cells per well. After 24 h of incubation, the medium was replaced with the prepared Oys-HAP extracts, followed by an additional 24 h incubation period. The toxicity of Oys-HAP was determined by measuring cell viability using a colorimetric assay with AlamarBlue reagent (Invitrogen, USA). The optical density (OD) was recorded at 540 nm wavelength using a spectrophotometer (Biotek Instruments, USA). All experiments were performed in triplicate. Samples were considered cytotoxic if the cell viability decreased by more than 30% relative to the untreated control. The cell viability was calculated using the equation below:

$$\text{Cell viability (\%)} = \frac{\text{Absorbance Sample} - \text{Absorbance Blank}}{\text{Absorbance Control} - \text{Absorbance Blank}} \times 100\% \quad (1)$$

The lowest toxic concentration (cell viability >70%) of each sample was selected for subsequent proliferation assays. The cells were seeded into 6 well plates at a density of 5×10^3 cells per well. Cell proliferation was monitored by measuring absorbance at predetermined time (Days 1, 3, 6, 9 and 12). The culture medium was replenished every three days throughout the experimental period. The negative control (culture medium) and positive control (DMSO) were included in both assays to enable comparison and validation of test methods.

2.10 Data and statistical analysis

The graphs and figures of physicochemical characterization including FTIR, XRD and SEM-EDX were generated using each built in instrument's software. The cytotoxicity and cell proliferation data were generated using GraphPad Prism 7.0 software. For the cell proliferation statistical analysis, the two-way ANOVA coupled with multiple comparison and Tukey post hoc test was used to compare each treatment group. Statistical significance was set at p-value of < 0.05.

3. Results and discussion

3.1 Physiochemical characteristics of prepared hydroxyapatite (HAP) powder from oyster shells

To the best of our knowledge, the present study was the first to synthesize HAP particles from oyster shells by using calcium carbonate and phosphoric acid as precursor materials via the hydrothermal route. The XRD was performed to confirm the phase composition, crystallinity and overall physical properties of the powder samples. The XRD result of different Oys-HAP powder preparation (RT, 1H, 6H and 24H) including the raw oyster shell powder is shown in Figure 1. All synthetic Oys-HAP powder showed diffraction sharp peaks which are characteristics to hydroxyapatite (HAP) with prominent reflections observed at approximately $2\theta = 25.9°, 31.7°, 32.9°, 34.0°, 39.8°, 46.7°$, and 49.5°, in correspondence to the peaks of (002), (211), (300), (202), (310), (222), and (213) planes respectively. All XRD patterns showed successful transformations to HAP.

Generally, low crystalline powder samples yield broadening of the XRD peaks [17]. The control wet precipitated RT sample which did not undergo the hydrothermal treatment yielded slightly low intensity diffraction peaks, which indicates poor crystallinity of 41.90%. When the treatment was introduced, it can be observed that the hydrothermal process improves the crystallinity of Oys-HAP samples. As the hydrothermal reaction time increases, the crystallinity of Oys-HAP improves respectively from 1H (55.0%) to 24H (70.4%) which is about 15.4% increase. Similarly, there was an increase of 15.4%. Increased crystallinity from 26.04% to 54.12% was observed when the hydrothermal reaction time increased from 10 min to 12 h [7]. A recent study also observed higher crystallinity observed when the temperature increased from 100°C to 200°C [18]. However, both studies did not perform the reaction above 12 h, which the 24 h treatment in the present study showed the highest crystallinity level (70.4%) in the present study. Accordingly, the hydrothermal methods can control HAP size, morphology and other properties [19]. Further, it is indicated that the growth of HAP crystals is strongly influenced by the reaction temperature [20].

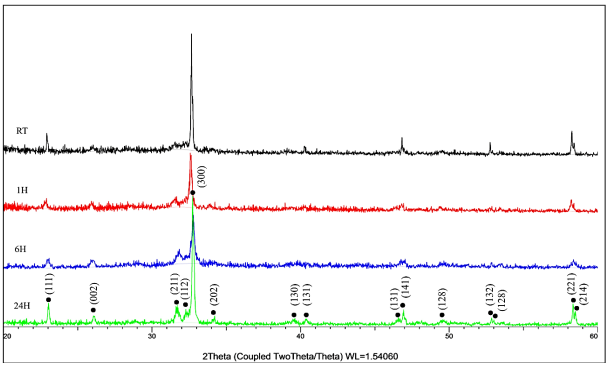

Figure 1. XRD pattern of 24H, 6H, 1H, RT.

The crystallite size was calculated using the Scherrer formula as shown in Table 2. It is observed that the hydrothermal treatment employed in the study from 1 h to 24 h did reduce the crystallite size of Oys-HAP samples ranging from 65.37 nm to 119.51 nm. The control RT sample showed the largest crystallite size of 119.51 in parallel with its low crystallinity. A larger crystallite size of HAP particles will reduce bone hardness [21].

As for the FE-SEM result, it was observed that the hydrothermal treatment did cause the Oys-HAP particles to become smaller. The particle size was reduced from RT (305.4 nm) to 24H (121.9 nm) which translates to about 60% reduction. However, it can be seen from SEM images that the powder contains various sizes and shapes of Oys-HAP particles. Briefly, RT sample consists of rod-shaped particles, 1H in slightly circular to oval shape particles, 6H in a mix of oval and elongated rod particles and 24H is similar to those in 6H. Similar morphology of HAP particles was seen produced using eggshells as precursor material [10]. Overall, Oys-HAP samples produced by present study forms nano scaled crystals. Collectively, it is like HAP in human bones [22]. Compared to larger sized particles, it has a larger surface area which can modulate better physiological functions. For instance, osteoblast functions were enhanced with the use of nHAP that selectively increased vitronectin protein absorption along with modulating overall osteoblast functions compared to bigger sized HAP [23].

The FTIR analysis of produced Oys-HAP powders produced at different hydrothermal reaction times is shown in Figure 3. The results of Oys-HAP are compared with the raw powder (OSP) to observe its transformations. The FTIR result demonstrated that all Oys-HAP samples synthesized in this study contain similar functional groups including Phosphate (PO_4^{3-}), Hydroxide (OH^-) and Carbonate (CO_3^{2-}). The absorption bands around 1637 cm^{-1} are attributed to the presence of water (H_2O) absorbed by the compound [24]. The phosphate bands at 961 cm^{-1}, 1017 cm^{-1}, and 1089 cm^{-1} were observed in all synthetic HAP samples. The prominent peaks at 1457 cm^{-1} and 1458 cm^{-1} are associated with the substitution of PO_4^{3-} groups by CO_3^{2-} which results in the formation of β-type carbonate HA [25]. This specific type of HAP mimics the human natural bone [26]. Carbonate (CO_3^{2-}) groups which were present in synthetic Oys-HAP powders in present study is also a component of apatite [27]. Further, the HAP powder samples showed a non-stoichiometric ratio of Ca/P (Table 2). However, better bioactivity and sintering quality have been observed compared to HAP with a stoichiometric ratio of 1.67 [28].

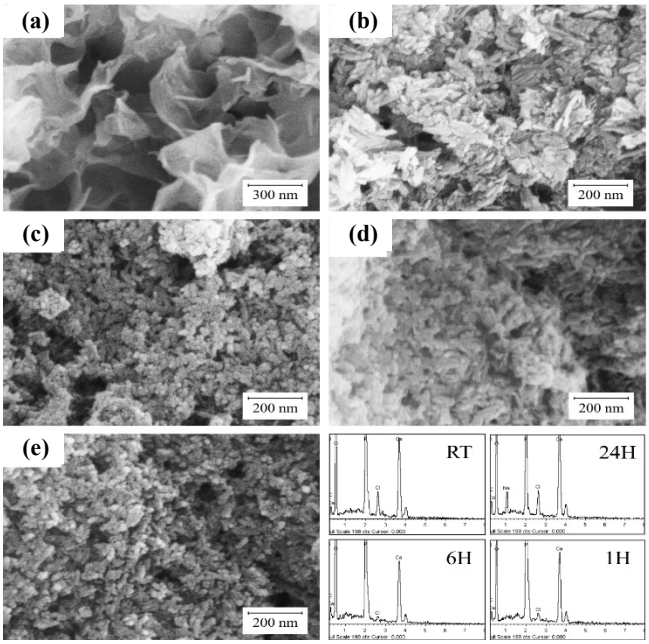

Figure 2. SEM micrographs and EDX analyses of powder samples at 20,000X (a) OSP, (b) RT, (c) 1H, (d) 6H, and e) 24H .

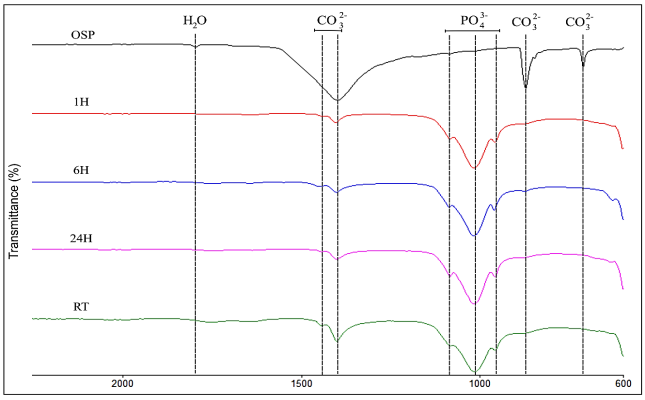

Figure 3. FTIR transmittance (%) of powder samples (OSP, 1H, 6H, 24H and RT).

Table 2. The specific calcium to phosphate ratio, crystallinity and crystallite size of powder samples.

Samples name/code	Ca [%]	P [%]	Ca:P ratio	Crystallinity [%]	Crystallite size [nm]
1H	34.56	15.82	2.18	55.0	65.37
6H	27.45	12.18	2.25	53.4	59.01
24H	31.80	13.16	2.41	70.4	60.72
RT	18.27	13.22	1.38	41.9	119.51

Table 3. BET analysis of powder samples.

Samples name/code	BET specific surface area [$m^2 \cdot g^{-1}$]	Total pore volume [$cm^3 \cdot g^{-1}$]	Average pore size [nm]
1H	34.16	0.2807	30.87
6H	35.50	0.2215	24.95
24H	41.34	0.2841	32.87
RT	22.22	0.0729	13.12
OSP	4.29	0.0133	12.37

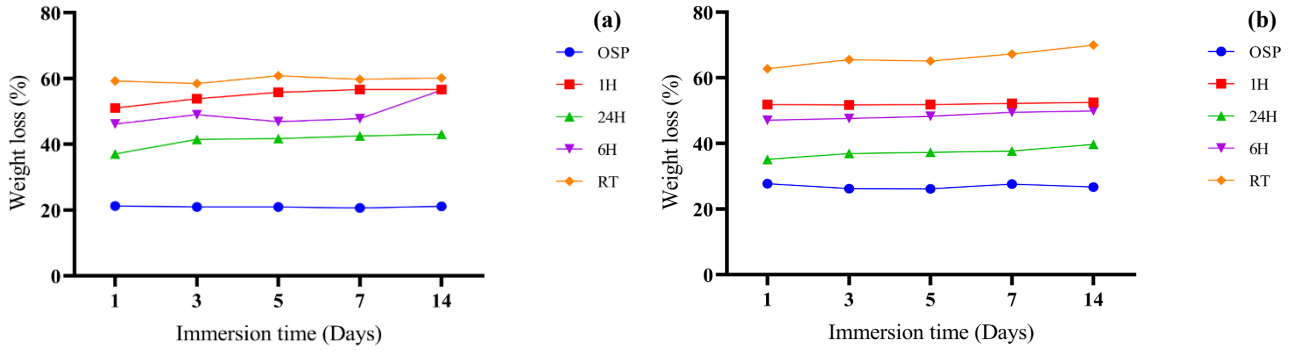

Figure 4. Biodegradation graph of powder samples OSP, 1H, 6H, 24H and RT; a) Phosphate Buffer Saline (PBS), b) Simulated Body Fluid (SBF).

3.2 Surface area characteristics

The textural and surface area properties of Oys-HAP samples were analyzed using the nitrogen adsorption-desorption isotherms method. The results are tabulated in Table 3. The specific surface area mainly ranges from 4.29 $m^2 \cdot g^{-1}$ to 35.50 $m^2 \cdot g^{-1}$. The 1H and 6H samples exhibited the highest surface area of 34.16 $m^2 \cdot g^{-1}$ and 35.50 $m^2 \cdot g^{-1}$ indicating a much smaller particle formed during the synthesis with a morphology structure. The 24H sample exhibited the highest surface area of 41.34 $m^2 \cdot g^{-1}$, indicating a much smaller particle formed during the synthesis.

The lowest surface area was displayed in the OSP sample of 4.29 $m^2 \cdot g^{-1}$ which suggests a much more dense and compacted particle structure. The total pore volume obtained using the BJH method showed a similar trend with the specific surface area result, ranging from 0.0133 $cm^3 \cdot g^{-1}$ to 0.2807 $cm^3 \cdot g^{-1}$. The highest pore volume was observed in a 24H sample followed by 6H, 1H and RT. Higher porosity of samples influences its fluid accessibility and exposure. The lowest pore volume of 0.013 $cm^3 \cdot g^{-1}$ was observed in the raw oyster shell powder (OSP) further suggesting its dense structure. The average pore size was also determined using the BJH method and ranged from 12.37 nm to 32.87 nm. The pore size also yielded a similar trend however, suggesting that all Oys-HAP powder samples possess mesoporous structures, characterized by the pore size that is in between 2 nm to 50 nm, described by IUPAC definition [29].

Generally, higher temperature during hydrothermal reactions promotes further activation of any particle surface enabling better ion exchange and crystal rearrangement [30]. The surface area of HAP is influenced by the total pore volume or its crystal size [31]. Previous studies had also stated the importance of surface area in producing biomaterial for bone tissue regeneration [32-34]. A higher surface area of HAP promotes better bone formation via the absorption of extracellular matrix proteins [35]. According to this study, hydrothermal treatment influenced the surface area properties of synthetic HAP powders. The specific surface area, pore size and volume increased as the reaction time increased.

3.3 Biodegradation evaluation

The degradation of HAP samples is important in predicting its long-term performance [36]. In this study, phosphate buffer saline (PBS) and simulated body fluid (SBF) were used to simulate a physiological environment. SBF contains supersaturated ions concentrations close to human blood plasma compared to PBS [14,37]. The use of two different solutions was to observe any differences in dissolution rates of powder samples. Figure 4 shows the degradation potential of OSP, 1H, 6H, 24H and RT accordingly. Overall, all samples showed similar results for degradation percentage in both PBS and SBF. An almost linear relationship between the immersion time and degradation rate was obtained in both solutions [38].

The highest percentage of degradation around 57% (PBS) and 68% (SBF) were shown by the RT sample in both immersion solutions. The slowest degradation was observed in the OSP sample with ~20% (PBS) and ~26% (SBF). This is probably due to the absence of P-O bond in the samples and the larger, less porous microstructure and integrity of the powder sample. Raw oyster shell powder largely contains calcium carbonate which is insoluble in water [39,40]. Successful transformation of raw oyster shell powder improved its solubility and bioavailability by increasing its surface area [41]. In contrast, Oys-HAP samples showed a better degradation rate. The fastest degradation was observed in the RT sample with ~60% (PBS) and ~68% (SBF). This is supported by its low crystallinity value of the sample as listed in Table 2. A steady rate of degradation was observed in samples 1H>6H>24H. The results shown in the present study exhibit a comparable degradation rate or weight loss compared to previous reports [18]. Despite the high porosity structure of the 24H Oys-HAP sample, it showed the lowest slowest degradation which was probably due to its high crystallinity.

Apart from crystallinity, grain size, microstructure and surface area of HAP powders directly affects its degradation [42]. As the degree of crystallinity increases, the samples degrade slower. Further, the degradation rate of HAP is also influenced by the physiological condition of the human body [43]. The degradation of HAP is important as it directly influences its bioactivity and biological responses [44]. Poor degradation rate will result in lowered ions such as Ca^{2+} concentration which in turn does not stimulate any cellular proliferation [45].

3.4 Biocompatibility test

Biocompatibility *in vitro* testing is a fast and inexpensive method to screen the toxicity of biomaterials. The indirect method utilizes material extract; the test item will be soaked in a physiological vehicle to extract any toxic leachable. The Saos-2 osteoblast-like cell line was used in this study to represent the bone tissue environment due to its mature phenotype. It is characterized to be the closest resemblance with Human Osteoblast (HOB) by its proliferation, overall phenotype

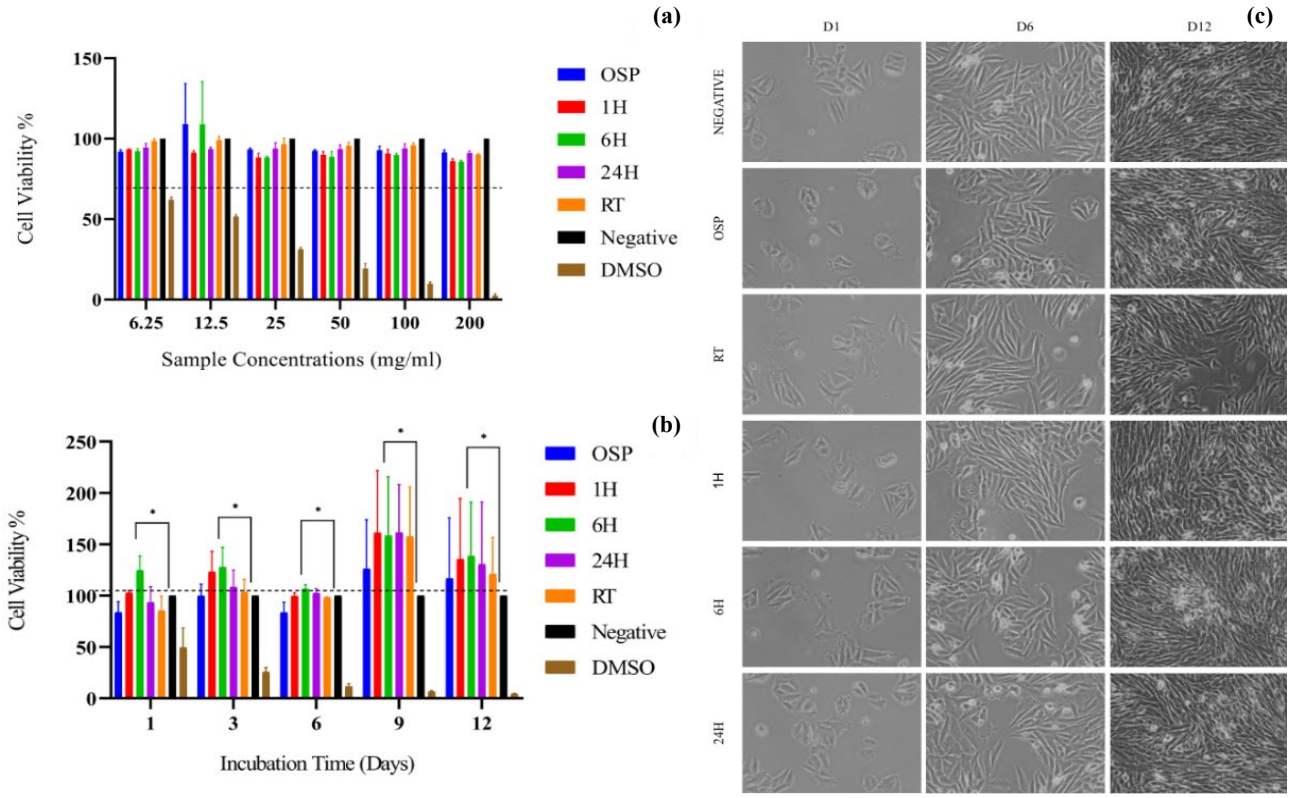

Figure 5. The cell viability and morphology results of Oys-HAP samples using the human osteoblast-like cell line (Saos-2) as an *in vitro* biocompatibility model. (a) Cytotoxicity, (b) Proliferation, (c) Cell morphology at 12.5 mg·mL^{-1} material extract treatment. The significance in cell proliferation data is *p<0.05 vs negative control.

and molecular functions [46]. The cytotoxicity of all powder samples was determined using the absorbance value of reduced resazurin dye after exposure to the sample extracts. According to ISO10993:5, the material or device is determined to be "non-toxic" if the percentage of cell viability after exposure is above 70% compared to the negative control [15].

Hydroxyapatite (HAP) is generally biocompatible, however, changes in synthesis methods which yield different forms of HAP still impose the need for biocompatibility assessments, especially for nano-sized HAP particles [9]. Overall, all Oys-HAP samples tested in the study showed no signs of toxicity against Saos-2 cells at the highest concentration of material extract, indicated by the percentage of viable cells after exposure shown in Figure 5. However, a slight increase of cell viability was observed in the 6H sample by ~10% from negative control. Previous studies indicated similar results despite the difference in synthesis methods and cell line use. Two recent studies tested HAP particles produced via the hydrothermal method against the MG-63 cell line. A direct contact viability assay performed by [7] yielded a marked optical density increase from the day 1 to day 7 culture and showed good cell attachment on HAP surface.
A steady proliferation pattern was observed in all Oys-HAP samples. A steady increase of cell viability upon incubation with treatment of material extract at 12.5 mg·mL^{-1}. All samples showed significant increase in cell viability on day 9. The highest cell viability of 165.6% was produced by sample 6H followed by 24H, RT, 1H, and OSP. Statistical significance ($p<0.05$) was observed in the 6H sample compared to the negative control. Saos-2 cell morphology was not altered upon increased incubation time with the extract. The Saos-2 culture showed normal polygonal and spindle-shaped morphology with well-defined membranes. The cells adhered to the plate surface well with a prominent nucleus. At 12 days, the cells reached confluency with flattened and overlapping clusters indicating a healthy culture with regards to the treatment.

4. Conclusions

Hydroxyapatite (HAP) powder samples were successfully synthesized by using the hydrothermal method using oyster shells as the main calcium source. The reaction time of 1H, 6H and 24H changed the physiochemical properties of the Oys-HAP powder particles and resulted in the reduction of the overall particle size, specific surface area and porosity. The in vitro biocompatibility assessment via cytotoxicity assay against Saos-2 osteoblast-like cell line showed non-toxic reaction of HAP powders making it viable for biomedical applications. Further, the cell proliferation assay showed the proliferative ability of HAP samples. The use of oyster shells as a precursor material showed an excellent alternative method to reduce the cost of producing high quality HAP.

Acknowledgements

This study is supported by New Industrial Master Plan 2030 NI254301 - NIMP CLINICAL-MD3: ADVANCED CLINICAL MIDPOINT (ACM) and "grant" at Medical Device Innovation Centre (MDIC), Advanced Materials Research Centre (AMREC), SIRIM Industrial Research, SIRIM Berhad, Malaysia.

References

[1] H. Gul, M. Khan, and A. S. Khan, "Bioceramics," in *Handbook of Ionic Substituted Hydroxyapatites*, Elsevier, 2020, pp. 53–83.

[2] P. Murray, "Biocompatibility of biomaterials for dental tissue repair," in *Biocompatibility of Dental Biomaterials*, Elsevier, 2017, pp. 41–62.

[3] R. P. K. Penttinen, "Cell interaction with bioactive glasses and ceramics," in *Bioactive Glasses, Elsevier*, 2018, pp. 145–180.

[4] K. M. Galler, F. P. Brandi, S. Kirchhof, and M. Widbiller, "Suitability of different natural and synthetic biomaterials for dental pulp tissue engineering," *Tissue Engineering Part A*, vol. 24, no. 3–4, pp. 234–244, 2017.

[5] M. Sadat-Shojai, M.-T. Khorasani, and A. Jamshidi, "Hydrothermal processing of hydroxyapatite nanoparticles—A Taguchi experimental design approach," *Journal of Crystal Growth*, vol. 361, pp. 73–84, 2012.

[6] G. Zhang, J. Chen, S. Yang, Q. Yu, Z. Wang, and Q. Zhang, "Preparation of amino-acid-regulated hydroxyapatite particles by hydrothermal method," *Materials Letters*, vol. 65, no. 3, pp. 572–574, 2011.

[7] S. C. Wu, H. C. Hsu, W. H. Wu, and W. F. Ho, "Enhancing bioactivity and mechanical properties of nano-hydroxyapatite derived from oyster shells through hydrothermal synthesis," *Nanomaterials (Basel)*, vol. 14, no. 15, 2024.

[8] R. A. Bapat, C. P. Joshi, P.Bapat, T. V. Chaubal, R. Pandurangappa, N. Jnanendrappa, B. Gorain, S. Khurana, and P. Kesharwani, "The use of nanoparticles as biomaterials in dentistry," *Drug Discovery Today*, vol. 24, no. 1, pp. 85–98, 2019.

[9] M. Motskin, D. M. Wright, K. Muller, N. Kyle, T. G. Gard, A. E. Porter, and J. N. Skepper, "Hydroxyapatite nano and microparticles: Correlation of particle properties with cytotoxicity and biostability," *Biomaterials*, vol. 30, no. 19, pp. 3307–3317, 2009.

[10] S. C. Wu, H. C. Hsu, H. F. Wang, S. P. Liou, and W. F. Ho, "Synthesis and characterization of nano-hydroxyapatite obtained from eggshell via the hydrothermal process and the precipitation method," *Molecules*, vol. 28, no. 13, 2023.

[11] C. M. Mardziah, S. Ramesh, M. F. Abdul Wahid, H. Chandran, A. Sidhu, S. Krishnasamy, and J. Purbolaksono, "Effect of zinc ions on the structural characteristics of hydroxyapatite bioceramics," *Ceramics International*, vol. 46, no. 9, pp. 13945–13952, 2020.

[12] E. Landi, A. Tampieri, G. Celotti, and S. Sprio, "Densification behaviour and mechanisms of synthetic hydroxyapatites," *Journal of the European Ceramic Society*, vol. 20, no. 14–15, pp. 2377–2387, 2000.

[13] S. Ibrahim, S. A. Bakar, N. S. K. Bashah, N. M. Zainon, S. Sabudin, A. Seeni, O. J. Ping, and N. Yahaya, "Cytocompatible carbonate apatite derived from gypsum granules for bone regeneration," *Malaysian Journal of Medicine and Health Sciences*, vol. 21, pp. 73–77, 2025.

[14] T. Kokubo and H. Takadama, "How useful is SBF in predicting in vivo bone bioactivity?," *Biomaterials*, vol. 27, no. 15, pp. 2907–2915, 2006.

[15] *Biological evaluation of medical devices Part 5: Tests for in vitro cytotoxicity* , ISO 10993-5:2009, Aug. 09, 2025. [Online]. Available: https://www.iso.org/standard/36406.html.

[16] *Biological evaluation of medical devices Part 12: Sample preparation and reference materials*, ISO 10993-12:2021, Aug. 09, 2025. [Online]. Available: https://www.iso.org/standard/75769.html.

[17] S. Ramesh, C. Y. Tan, R. Tolouei, M. Amiriyan, J. Purbolaksono, I. Sopyan, and W. D. Teng, "Sintering behavior of hydroxyapatite prepared from different routes," *Materials & Design*, vol. 34, pp. 148–154, 2012.

[18] S.-C. Wu, H.-C. Hsu, L.-C. Ou, and W.-F. Ho, "Effects of hydrothermal temperature on the synthesis and characterization of bioactive hydroxyapatite nanoparticles from oyster shell," *Journal of the Australian Ceramic Society*, vol. 61, no. 4, pp. 1525–1536, 2025.

[19] V. R. Sivaperumal, R. Mani, M. S. Nachiappan, and K. Arumugam, "Direct hydrothermal synthesis of hydroxyapatite/alumina nanocomposite," *Materials Characterization*, vol. 134, pp. 416–421, 2017.

[20] A. Yelten-Yilmaz and S. Yilmaz, "Wet chemical precipitation synthesis of hydroxyapatite (HA) powders," *Ceramics International*, vol. 44, no. 8, pp. 9703–9710, 2018.

[21] C. Chappard, G. André, M. Daudon, and D. Bazin, "Analysis of hydroxyapatite crystallites in subchondral bone by Fourier transform infrared spectroscopy and powder neutron diffraction methods," *Comptes Rendus Chimie*, vol. 19, no. 11–12, pp. 1625–1630, 2016,

[22] T. J. Webster, C. Ergun, R. H. Doremus, R. W. Siegel, and R. Bizios, "Enhanced osteoclast-like cell functions on nanophase ceramics," *Biomaterials*, vol. 22, no. 11, pp. 1327–1333, 2001.

[23] A. Pataquiva Mateus, F. J. Monteiro, and M. Pía Ferraz, "Nanoparticles of hydroxyapatite: Preparation, characterization and cellular approach - An overview," *Revista Mutis*, vol. 3, no. 2, pp. 43–56, 2013.

[24] J. P. Lafon, E. Champion, and D. Bernache-Assollant, "Processing of AB-type carbonated hydroxyapatite $Ca_{10-x}(PO_4)_{6-x}(CO_3)_x(OH)_{2-x-2y}(CO_3)_y$ ceramics with controlled composition," *Journal of the European Ceramic Society*, vol. 28, no. 1, pp. 139–147, 2008.

[25] A. I. Bucur, R. A. Bucur, Z. Szabadai, C. Mosoarca, and P. A. Linul, "Influence of small concentration addition of tartaric acid on the 220°C hydrothermal synthesis of hydroxyapatite," *Materials Characterization*, vol. 132, pp. 76–82, 2017.

[26] T. Tolga Demirtaş, G. Kaynak, and M. Gümüşderelioğlu, "Bone-like hydroxyapatite precipitated from 10×SBF-like solution by microwave irradiation," *Materials Science and Engineering: C*, vol. 49, pp. 713–719, 2015.

[27] R. Z. LeGeros, "Calcium phosphate-based osteoinductive materials," *Chemical Reviews*, vol. 108, no. 11, pp. 4742–4753, 2008,

[28] I. R. Gibson, and W. Bonfield, "Novel synthesis and characterization of an AB-type carbonate-substituted hydroxyapatite," *Journal of Biomedical Materials Research*, vol. 59, no. 4, pp. 697–708, 2002.

[29] K. Ariga, A. Vinu, Y. Yamauchi, Q. Ji, and J. P. Hill, "Nanoarchitectonics for mesoporous materials," Bulletin of the Chemical Society of Japan, vol. 85, no. 1, pp. 1–32, 2012.

[30] W. Liang, Y. Niu, S. Ge, S. Song, J. Su, and Z. Luo, "Effects of hydrothermal treatment on the properties of nanoapatite crystals," *International Journal of Nanomedicine*, vol. 7, pp. 5151–5158, 2012.

[31] L. Yin, X. Xu, C. Chu, P. Lin, H. Huang, B. Luo, and C. Yang, "In-vitro characterization and evaluation of mesoporous titanium dioxide composite hydroxyapatite and its effectiveness in occluding dentine tubules," BMC Oral Health, vol. 22, Art. no. 43, 2022.

[32] P. Habibovic, M. C. Kruyt, M. V. Juhl, S. Clyens, R. Martinetti, L. Dolcini, N. Theilgaard, and C. A. van Blitterswijk, "Comparative in vivo study of six hydroxyapatite-based bone graft substitutes," *Journal of Orthopaedic Research*, vol. 26, no. 10, pp. 1363–1370, 2008.

[33] M. Bohner, "Calcium orthophosphates in medicine: From ceramics to calcium phosphate cements," Injury, vol. 31, pp. D37–D47, 2000.

[34] N. Patel, I. R. Gibson, S. Ke, S. M. Best, and W. Bonfield, "Calcining influence on the powder properties of hydroxyapatite," *Journal of Materials Science: Materials in Medicine*, vol. 12, no. 2, pp. 181–188, 2001.

[35] M. Rouahi, E. Champion, O. Gallet, A. Jada, and K. Anselme, "Physico-chemical characteristics and protein adsorption potential of hydroxyapatite particles: Influence on in vitro biocompatibility of ceramics after sintering," *Colloids and Surfaces B: Biointerfaces*, vol. 47, no. 1, pp. 10–19, 2006.

[36] N. Suresh, V. K. Sweety, N. Suresh, A. R. Suraj, T. Waltimo, and S. Anil, "NATURAL sources of hydroxyapatite for biomedical applications," *Ceramics International*, vol. 52, no. 2, pp. 1383–1391, 2025.

[37] Y. Ebisawa, T. Kokubo, K. Ohura, and T. Yamamuro, "Bioactivity of $CaO{\cdot}SiO_2$-based glasses:in vitro evaluation," *Journal of Materials Science: Materials in Medicine*, vol. 1, no. 4, pp. 239–244, 1990.

[38] Y. Wang, W. He, H. Hao, J. Wu, and N. Qin, "Eggshell derived Se-doped HA nanorods for enhanced antitumor effect and curcumin delivery," *Journal of Sol-Gel Science and Technology*, vol. 87, no. 10, pp. 600–607, 2018.

[39] J. Malešič, M. Kadivec, M. Kunaver, T. Skalar, and I. K. Cigić, "Nano calcium carbonate versus nano calcium hydroxide in alcohols as a deacidification medium for lignocellulosic paper," *Heritage Science*, vol. 7, no. 1, p. 50, 2019.

[40] W. E. Olds, D. C. W. Tsang, and P. A. Weber, "Lignite-derived humic substances for treatment of acid mine drainage," *Environmental Engineering Science*, vol. 30, no. 10, pp. 638–645, 2013.

[41] S. Ahn, S. Lee, and S. Lim, "Antimicrobial properties of thermally processed oyster shell powder for use as calcium supplement," *Foods*, vol. 14, no. 15, p. 2579, 2025.

[42] R. Nithya, and N. Meenakshi Sundaram, "Biodegradation and cytotoxicity of ciprofloxacin-loaded hydroxyapatite-polycaprolactone nanocomposite film for sustainable bone implants," *International Journal Nanomedicine*, vol. 10, no. Sup 2, pp. 119–127, 2015.

[43] V. Ganesan, M. Devaraj, S. K. Govindan, V. S. Kattimani, and G. Easwaradas Kreedapathy, "Eggshell derived mesoporous biphasic calcium phosphate for biomedical applications using rapid thermal processing," *International Journal of Applied Ceramic Technology*, vol. 16, no. 5, pp. 1932–1943, 2019.

[44] S. Palakurthy, P. A. Azeem, K. Venugopal Reddy, V. Penugurti, and B. Manavathi, "A comparative study on in vitro behavior of calcium silicate ceramics synthesized from biowaste resources," *Journal of the American Ceramic Society*, vol. 103, no. 2, pp. 933–943, 2019.

[45] S. Palakurthy, V. G. R. K, R. K. Samudrala, and A. A. P, "*In vitro* bioactivity and degradation behaviour of β-wollastonite derived from natural waste," *Materials Science and Engineering: C*, vol. 98, pp. 109–117, 2019.

[46] E. M. Czekanska, M. J. Stoddart, J. R. Ralphs, R. G. Richards, and J. S. Hayes, "A phenotypic comparison of osteoblast cell lines versus human primary osteoblasts for biomaterials testing" *Journal of Biomedical Materials Research Part A*, vol. 102, no. 8, pp. 2636–2643, 2014.